Collisional tectonics of the Baltic Shield in the northern Gulf of Bothnia from seismic data of the BABEL project

Karsten Gohl* and Laust B. Pedersen

Department of Geophysics, Solid Earth Physics, Uppsala University, Box 556, S-75236 Uppsala, Sweden

SUMMARY

Densely spaced wide-angle data from stations recording airgun shots along BABEL profile 2 in the northern Gulf of Bothnia were analysed, modelled, and compared with the normal-incidence recordings. Profile 2 extends from the metasedimentary and metavolcanic Proterozoic Central Svecofennian Province into the volcanic Northern Svecofennian Province of magmatic arc affinity and crosses the Proterozoic–Archaean boundary of the northern Baltic Shield as defined from isotope studies. We used a 2-D traveltime inversion to derive P- and S-wave velocity–depth models and a distribution of Poisson's ratios along the profile.

A series of north-dipping wide-angle reflectors characterize the middle and lower crust in the southern part of the model, coinciding with similar events in previous multichannel wide-angle data and the CMP recordings. Several subhorizontal upper to mid-crustal wide-angle reflectors and a well-resolved Moho boundary at 42 to 45 km depth coincide with reflective zones or changes in reflectivity patterns of the CMP data. P-wave velocities increase from $5.7\,\text{km s}^{-1}$ at the near-surface to 6.4 and $6.6\,\text{km s}^{-1}$ in the mid-crust and up to $7.6\,\text{km s}^{-1}$ in the lowermost crust. P_n velocities reach 8.0 to $8.2\,\text{km s}^{-1}$ below the Moho in the northern part of the model but are less than $8.0\,\text{km s}^{-1}$ in the southern part. Poisson's ratios, calculated from the P- and S-wave models, range from 0.21 to 0.25 in the uppermost crust to about 0.30 in the lower crust and upper mantle. Our velocity and Poisson's ratio models indicate that the upper crust contains predominantly felsic, quartz-rich rocks. The increase of P-wave velocity and Poisson's ratio in the mid- to lower crust is explained by increasingly mafic composition.

We propose a geological model across the northern Gulf of Bothnia that combines our velocity–depth model with results from the seismic normal-incidence experiment, previous geophysical information, and geological surface observations. The model consists of a possibly multiple Proterozoic north-dipping subduction zone with remnants of oceanic crust and zones of imbricated metasediments and mafics on top. There is evidence for a metasedimentary fore-arc basin in the middle crust and a layer of mafic to ultramafic cumulates at the base or below parts of the lower crust. South-dipping mid- and lower crustal zones of high reflectivity in the northern part of profile 2 indicate that Archaean crust underlies the Northern Svecofennian Province. The major features of this Proterozoic collision zone, such as the suggested subduction slab, zones of crustal reflectors dipping parallel to the slab, a metasedimentary basin, and mafic to ultramafic cumulates between the subduction slab and overlaying Moho, are well-preserved analogues of recent oceanic–continental collision and subduction zones.

Key words: Precambrian crust, subduction, traveltime inversion, wide-angle data.

*Now at: Alfred Wegener Institute for Polar and Marine Research, Postfach 120161, D-27515 Bremerhaven, Germany.

1   INTRODUCTION

The question of how plate tectonic principles and consequences were effective during the Precambrian has long been discussed extensively. Large-scale intracratonic fault and shear zones show evidence for Archean and early Proterozoic horizontal plate movements (i.e. Windley 1984). Large areas of Proterozoic crust have been interpreted as remnants of accreted magmatic arc complexes that contributed significantly to continental growth (Meissner 1986). An ideal field to study the structure of a Proterozoic–Archaean terrane boundary and the formation of its adjacent Proterozoic magmatic arc complex is the northern Gulf of Bothnia (Bothnian Bay) area in the Baltic Shield of Scandinavia. As part of the BABEL (*BA*ltic and *B*othnian *E*choes from the *L*ithosphere) experiment, deep crustal seismic normal-incidence (CMP) profiles were acquired in the Gulf of Bothnia and accompanied by simultaneous large-offset recordings of the airgun array (BABEL Working Group 1990, 1991, 1993). Due to continuous recordings from numerous instruments placed on exposed bedrock surrounding the Gulf, the seismic wavefield was densely sampled and high-quality data were obtained. Recent publications by the BABEL Working Group (1990, 1991, 1993) describe the main characteristics of the reflection data in the Bothnia Bay and give evidence for a Proterozoic subduction event in the deep crust and mantle. Following a preliminary interpretation of the *P*-wave wide-angle data (Gohl & Pedersen 1992), we evaluate in this study the *P*-wave and *S*-wave wide-angle reflection and refraction recordings of profile 2 and compare the results from a 2-D traveltime inversion with reflectivity patterns of the CMP profile. A geological model across the Bothnian Bay is suggested that might explain the collisional features interpreted from the geophysical data and geological surface observations.

2   GEOLOGY AND TECTONIC MODELS

The central Baltic Shield represents an assemblage of Archaean and Proterozoic blocks bounded by the Caledonide thrust belt to the west and south-west. These blocks or domains were formed by several orogenies, each of which is identified by its distinct sedimentary, magmatic and metamorphic characteristics (Gaál & Gorbatschev 1987; Gorbatschev & Gaál 1987). The regional geology is well described by Berthelsen (1984), Gaál (1986), Gaál & Gorbatschev (1987) and Gorbatschev & Gaál (1987), and summarized in a paper by the BABEL Working Group (1993). We describe the geological implications following from our seismic interpretation and a geological model for the northern Gulf of Bothnia.

BABEL profiles 2, 3 and 4 (Fig. 1) cross parts of the Central and Northern Svecofennian Provinces (CSP and NSP) in the proximity of the northbound Archaean block. The CSP consists of mainly 1.90 to 1.87 Ga old metagreywackes and metapelites with some tholeiitic basalts and ultramafic volcanics (Gorbatschev & Gaál 1987) and is bounded to the north by the volcanic belt of the NSP. The volcanics of the NSP are calc-alcaline dominated by rhyolites and dacites and interbedded with carbonates and epiclastic sediments (Gorbatschev & Gaál 1987). Thick

layers of basal greywackes suggest an original continental margin (Lundström 1987). Archaean components found in Proterozoic granites of the NSP suggest an underlying Archaean crust (Patchett, Todt & Gorbatshev 1987; Park 1991). Öhlander *et al.* (1993) show new results from Sm–Nd isotope analyses of Proterozoic granitoids and metavolcanites placing the Archaean palaeoboundary *c.* 100 km north of the Skellefte sulphide ore district in Sweden with a WNW strick direction (Fig. 1). The Skellefte district contains major components of marine calc-alkaline metavolcanites and is suggested to be the remnant of a volcanic arc (i.e. Claesson 1985). Rasmussen, Roberts & Pedersen (1987) detected a north-dipping zone of high conductivity underneath the Skellefte district from magnetotelluric measurements. North of the Skellefte district, large areas with terrestrial Arvidsjaur porphyries serve as another indication of an active continental margin (Lundberg 1980; Öhlander *et al.* 1993). Öhlander *et al.* (1993) correlate the volcanic Vihanti–Pyhäsalmi (VP) district of Finland with the north-west striking Skellefte district of Sweden, but there is an offset of several tenths of kilometres and a rotation in strike direction from NW to WNW in the Gulf of Bothnia between the zones. Both districts form the transition between the CSP and NSP. A north-west striking major tectonic shear zone, the Ladoga–Bothnian Bay (LBB) zone (also the Raahe–Ladoga zone), contains thrust nappe displacements in the order of tens of kilometres in Finland (Korsmann 1988). Mafic and ultramafic imbricated rocks within the LBB zone indicate obducted ophiolites associated with a subduction zone (Gorbatschev & Gaál 1987). The LBB zone does not have an equivalent with a similar strike direction in Sweden. A major fracture system, the Baltic–Bothnian megashear, runs parallel to the Swedish coast in a NNE direction in the Bothnian Bay west of profile 2 (Berthelsen 1984; Öhlander *et al.* 1993). The offset and rotation of strike direction between the Skellefte and the VP districts and the location of the megashear indicate horizontal-tectonic activities in the northern Gulf of Bothnia. A subduction zone is further suggested by the abundance of emplaced gabbroic to granite-dioritic and granitic plutons in the Svecofennian (Patchett *et al.* 1987). Front & Nurmi (1987) and Patchett *et al.* (1987) describe several phases of Svecofennian plutonism from 1.89 to 1.70 Ga, suggesting more than one collisional event.

3   SEISMIC WIDE-ANGLE DATA OF BABEL PROFILE 2

In our wide-angle analysis of shot profile BABEL 2, we used vertical and horizontal components of the Swedish stations 201, 203, 206 and the Finnish station F05 (Fig. 1). The airgun source array was fired every 62.5 m and recorded simultaneously by a 120 channel streamer and seismic instruments on land. Parameters of source array and CMP recordings are described in BABEL Working Group (1993). Stations 203 and 206 consisted of GDAS-seis instruments. Station 201 was a PC-based seismic recording system, and a PCM recorder was used on station F05. All instruments recorded vertical and two horizontal components. Former, traditional refraction surveys in the area had source and/or receiver spacings (trace spacing of source and/or receiver gathers) in the order of kilometres (i.e. Hirschleber *et al.*
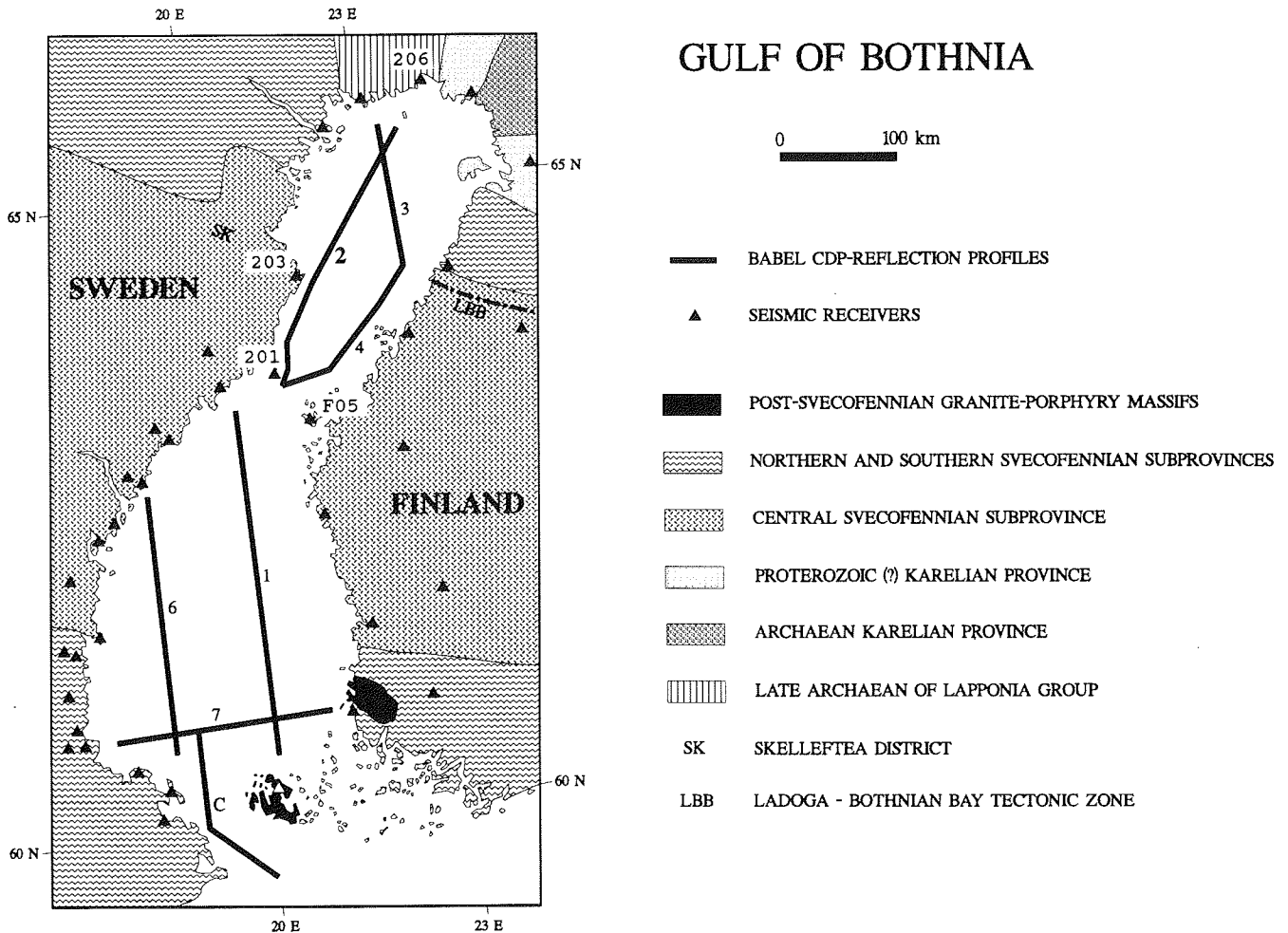
GULF OF BOTHNIA

0   100 km

▬▬▬   BABEL CDP-REFLECTION PROFILES

▲   SEISMIC RECEIVERS

■■■■   POST-SVECOFENNIAN GRANITE-PORPHYRY MASSIFS

▨▨▨▨   NORTHERN AND SOUTHERN SVECOFENNIAN SUBPROVINCES

▨▨▨▨   CENTRAL SVECOFENNIAN SUBPROVINCE

▭▭▭▭   PROTEROZOIC (?) KARELIAN PROVINCE

▨▨▨▨   ARCHAEAN KARELIAN PROVINCE

▥▥▥▥   LATE ARCHAEAN OF LAPPONIA GROUP

SK   SKELLEFTEA DISTRICT

LBB   LADOGA - BOTHNIAN BAY TECTONIC ZONE

Figure 1. Geological overview map of the Gulf of Bothnia region (northern-central Scandinavia) including BABEL seismic reflection profiles and locations of seismic landstations (triangles). Stations used in this paper are annotated. Geological features are outlined after Gorbatschev & Gaál (1987).

1975; Henkel, Lee & Lund 1990; Guggisberg, Kaminski & Prodehl 1991). The dense shot spacing of the wide-angle recordings in the BABEL project enabled us to perform processing sequences known from CMP reflection work such as trace stacking, deconvolution, and 2-D filtering. In revealing more coherent seismic phases over large distances, despite varying and decreasing amplitudes, the dense recording shows its major advantage.

The dominant signal frequency ranged between 7 and 9 Hz, with smaller harmonics at 15 to 17 Hz and 23 to 25 Hz. We bandpass-filtered (5–25 Hz) and deconvolved the traces of all receiver gathers. A predictive deconvolution operator with an operator length of 1000 ms, a prediction lag of 125 ms for the vertical component and 250 ms for the horizontal components, and an application gate starting at the onset of the first arrival removed most of the reverberations generated by the airgun bubble effect and sea-bottom multiples. To better display low-amplitude phases, we applied an automatic gain control (AGC) with a window length of 3000 ms.

All vertical component recordings show strong, dominant first P-wave arrivals (P_g) with apparent velocities between 5.7 km s^{-1} s at near-offset and 6.0 km s^{-1} at about 100 km

offset (Figs 2a–d). At farther offsets, the first-arrival velocities increase to values of 6.5 km s^{-1}, indicating arrivals of refracted or diving waves from the middle crust. In recordings of stations F05 and 206, the first arrivals at offsets greater than 200 km occur with apparent velocities between 7.8 and 8.2 km s^{-1}, suggesting refracted or diving wave phases from the lowermost crust and/or upper mantle (P_n). A second dominant phase that occurs in all recordings has a hyperbolic shape with largest amplitudes at offsets greater than 140 km. We identified this phase as a reflection from the Moho (P_mP). In some cases, this phase is continuous over large distances, for instance, from 100 to 260 km in recordings from station 206 (Fig. 2a). In the northern section of recordings from station 203 (Fig. 2b), the P_mP can already be traced at 75 km offset. All recordings contain numerous mid-crustal reflections that are less continuous and less consistent in their time–distance location from one station to another than the dominant phases. A striking feature, though, is the occurrence of a series of coherent phases with large move-outs at small offsets from recording stations F05 and 201 (Figs 2c and d). Their large two-way traveltime and move-out suggest that they originate from north-dipping mid- to lower crustal reflectors. Such north-dipping,
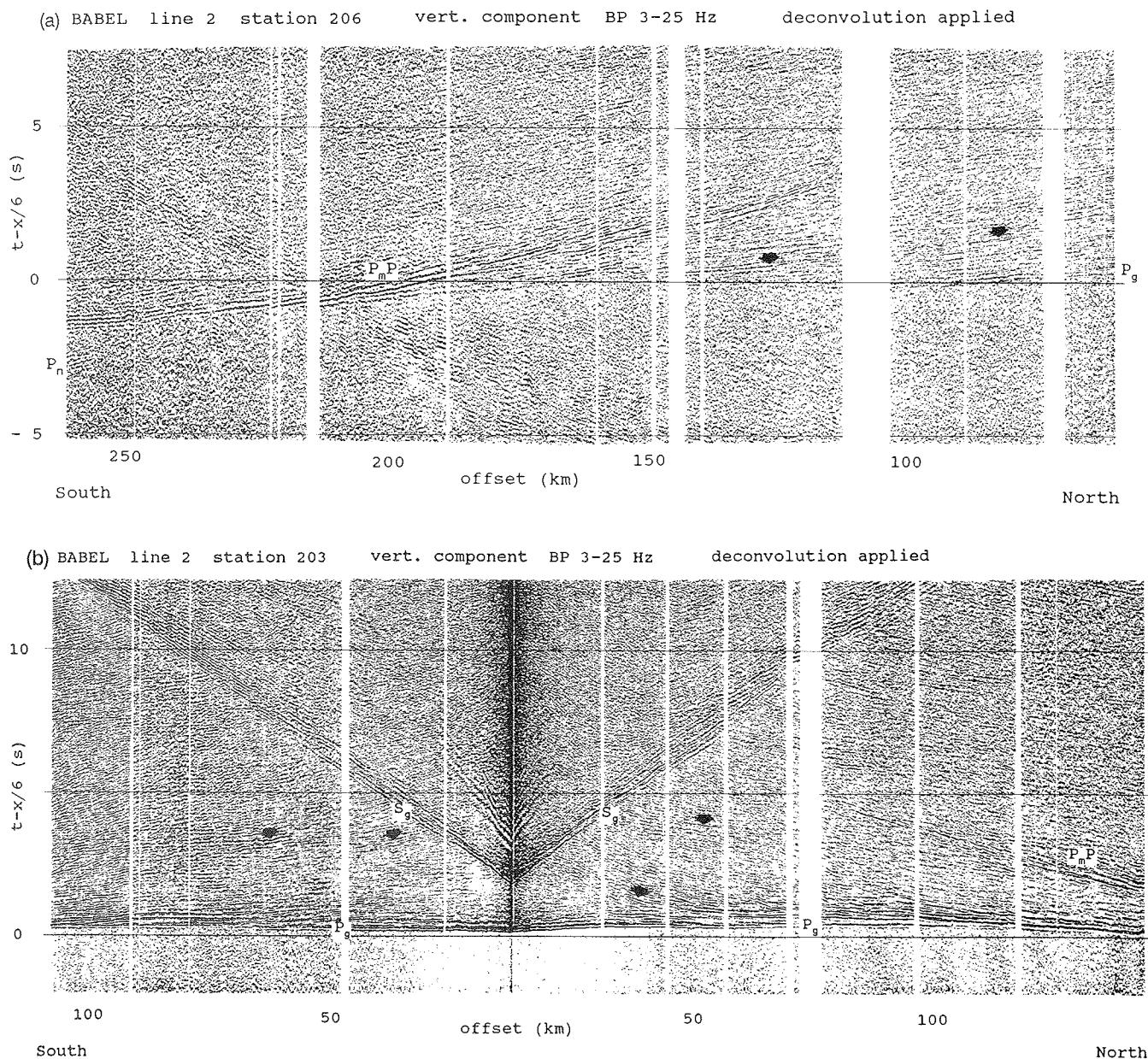
(a) BABEL line 2 station 206   vert. component BP 3-25 Hz   deconvolution applied

(b) BABEL line 2 station 203   vert. component BP 3-25 Hz   deconvolution applied

Figure 2. Seismic wide-angle recordings of BABEL shot-profile 2. The recordings contain filtered (3–25 Hz) and deconvolved traces. Large-amplitude first arrivals (P_g, S_g), Moho reflections (P_mP, S_mS) and an upper mantle diving phase (P_n) are annotated. The arrows indicate mid-crustal reflections. Shown are vertical components of stations (a) 206, (b) 203, (c) 201 and (d) F05, and (e) horizontal components (N–S) of station 201.

high-amplitude reflectors were also observed with a higher resolution from a multichannel array (station 202) close to station 201 (Lindsey & Snyder 1992).

The signal-to-noise ratio of observed S-wave arrivals in the horizontal components is generally lower than for P-wave arrivals. The deconvolution process removed most of the reverberations and multiples, but was not as successful as for P-wave phases. Most S-wave phases appear in bands broader than for the P-waves, mainly due to the lower velocities for S-wave energy. In an example of the recordings of the horizontal components (Fig. 2e), we identified S-wave first arrivals (S_g) and Moho reflections (S_mS) as dominant phases. Apparent first-arrival velocities

range from $3.4\,\text{km}\,\text{s}^{-1}$ at nearest offsets to more than $4.3\,\text{km}\,\text{s}^{-1}$ at farther distances. S_n phases with velocities of 4.2 to $4.4\,\text{km}\,\text{s}^{-1}$ are observed in recordings from stations F05 and 206. All recordings show mid-crustal reflections with low coherency and continuity. Recordings from stations F05 and 201 (Fig. 2e) contain mid- to lower crustal S-wave reflections from north-dipping interfaces.

4 2-D INVERSION

After a satisfactory phase correlation and identification was decided upon, a velocity–depth model could be obtained from the observed traveltime picks. In this study, we used a

(c) BABEL line 2 station 201 vert. component BP 3-25 Hz deconvolution applied
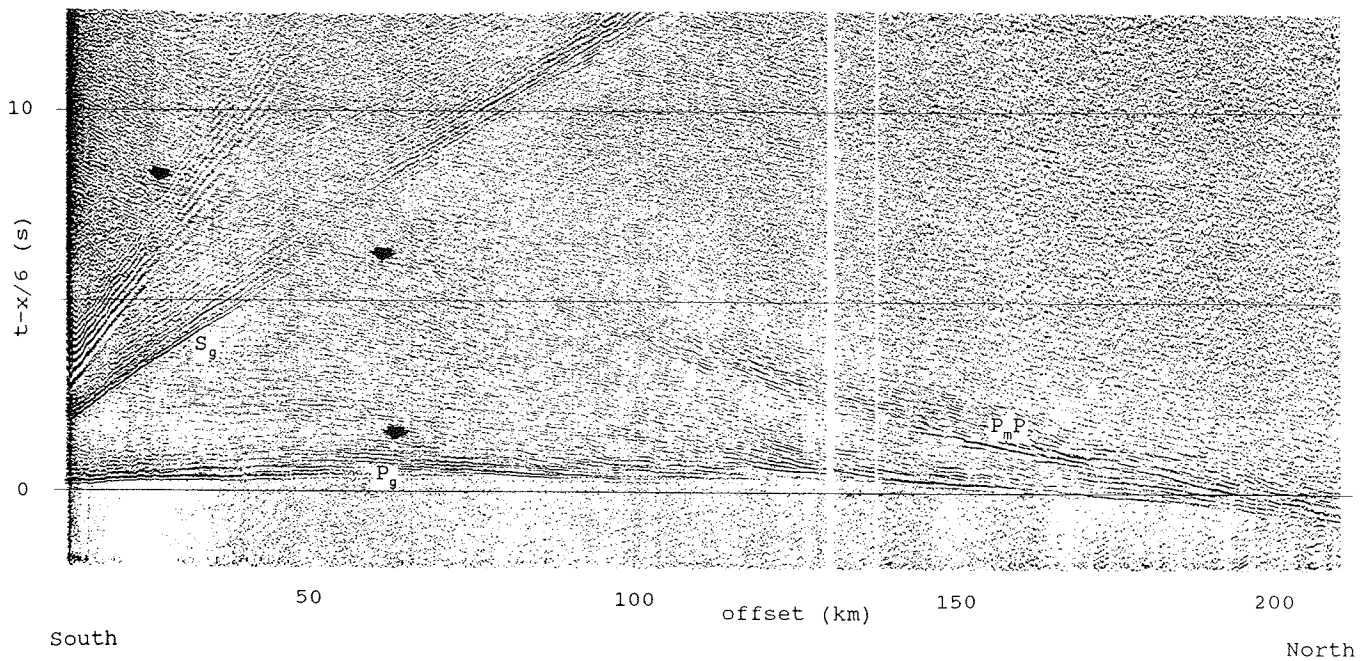
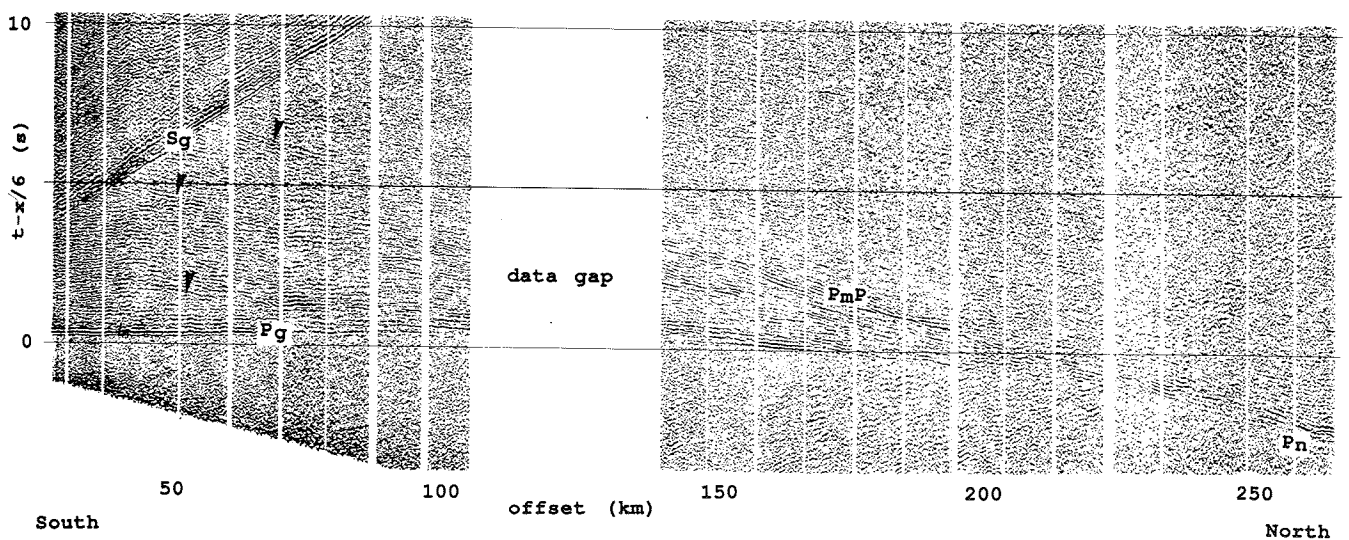(d) **BABEL** **line 2** **station F05** **vert. component** **BP 3-25 Hz** **deconvolution applied**

Figure 2. (*Continued*).

2-D traveltime inversion (Zelt & Smith 1992) to derive a general velocity–depth model of the crust along profile 2. The aim of the inversion process is to determine a model that minimizes the difference between observed and calculated data, which here are traveltimes. As opposed to standard forward modelling, an inversion provide estimates of model parameter uncertainties as well as their resolution. The iterative character of the method applied in this study involves adjustments of model parameters by applying a damped least-squares inversion of traveltimes (Zelt & Smith 1992). The model was parameterized by a set of layers broken into trapezoidal blocks (Fig. 3) with velocities linearily interpolated between nodes. We chose a horizontal block size of between 20 and 50 km, depending on the data density and quality; in other words, the sum of rays shot through a model region as well as the uncertainty in picking phases. Block boundaries were smoothed to avoid scattering and focusing effects of rays. As opposed to two-point ray tracing, this method uses an automatic calculation of take-off angles (Zelt & Ellis 1988). To quantitatively evaluate the best-fitted model, RMS traveltime residuals and parameter resolution are calculated allowing estimation of model reliability with respect to observed data. The stability of the inversion scheme is increased by reducing the number of independent model parameters, i.e. by keeping the velocity gradient or layer thickness fixed or by maintaining a
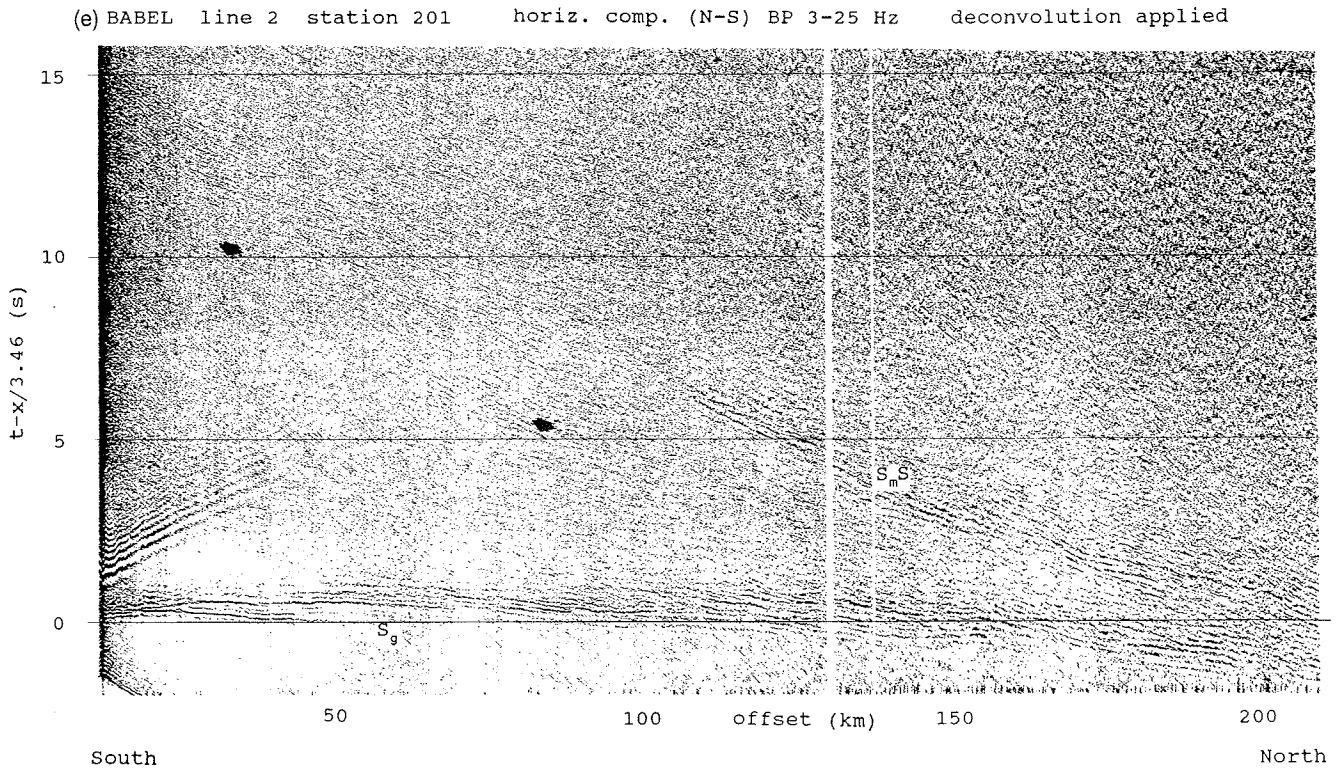
(e) BABEL line 2 station 201   horiz. comp. (N-S) BP 3-25 Hz   deconvolution applied

Figure 2. (*Continued*).

constant velocity discontinuity across a layer boundary, if there is evidence for that in the data. We applied the inversion as a layer-stripping technique in which we first inverted for the uppermost crust, then inverted arrivals from the middle and lower crust keeping the parameters of overlying layers fixed. The resolution of velocity and boundary nodes was finally calculated by taking the diagonal elements of the resolution matrix. This quantitative estimation of uncertainties is best used in a relative and not an absolute sense, and does not take into account 3-D effects, misidentification of phases and an insufficient block size parameterization of the model by neglecting fine heterogeneities (Zelt & Smith 1992).

4.1 *P*-wave model

In a 2-D theoretical case with ideal data, a linearized 2-D inversion may often invert for a velocity–depth model
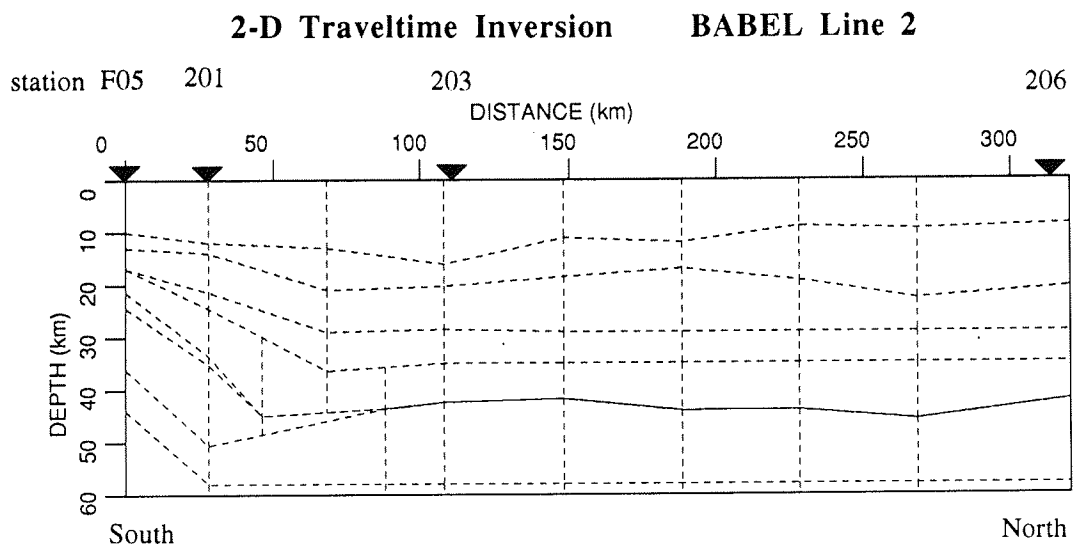

Figure 3. Trapezoidal block parameterization of final velocity–depth model for 2-D traveltime inversion. Velocities between corner points are linearily interpolated (Zelt & Smith 1992). The triangles indicate locations of recording stations used to derive the final model. For the iterative modelling process, layer boundaries are smoothed to avoid scattering and focusing of rays (not shown in figure).

independent of varying initial models. In our case, as in most crustal-scale wide-angle reflection and refraction surveys, however, neither the shot–receiver geometry nor the strike of geological features are strictly 2-D. Therefore, we generated an initial model by using simple forward ray tracing. After comparing traveltime-offset pairs of *P*-wave phases among all recordings, we grouped the identified reflection phases to implement six initial horizontal layers. The initial layer thicknesses were based on simple 1-D depth estimates from principal wide-angle reflections and refractions. We implemented a general crustal velocity distribution for the initial model. Because of the observation of the large move-out mid- to lower crustal reflections from stations F05 and 201 (Figs 2d and e), we added north-dipping interfaces in the southern part of the initial model. Later testing showed, however, that the implementation of dipping interfaces in the starting model was not necessary but that the inversion iterations resulted in layers with similar dip angles and depths as resulted from using a starting model with dipping interfaces. We started inverting traveltimes of the first arrivals and proceeded with later reflection and refraction phases. The traveltime-offset pairs were assigned uncertainties in time between 0.1 and 0.2 s corresponding to confidence in picking phase onsets. The inversion routine converged to minima of rms traveltime residuals after two or three iterations for each layer by simultaneously inverting for velocities and depths. Generally, the inversion remained stable despite deviation of the source–receiver geometry from two dimensions. This indicates that geological boundaries striking perpendicular to profile 2 are dominant. Only in a few boundary and velocity nodes did parameters reach unreasonable values, which had to be corrected manually and kept constant for subsequent iterations. We were able to fit most of the calculated traveltime curves within the uncertainty bounds of the observed traveltimes (0.1–0.2 s). The fit was particularly good for most of the north-dipping reflectors of the southern part and the P_mP and P_n phrases (Figs 4a and b).

We calculated a section of synthetic amplitudes for recording station 203 in order to compare with the observed non-normalized seismograms (Figs 5a and b). The relative amplitude distribution is satisfactory for the P_mP and some upper to mid-crustal reflections. Our velocity–depth model, however, represents a rather simplified crustal section with first-order discontinuities. To account for a possibly more complex interface structure, a detailed wavefield study of a particular area would be necessary, which was not the intention of this paper.

Through the iterative optimization process the final velocity and depth nodes for each layer changed significantly in parts of the model such as the zone of dipping reflectors, the Moho geometry and the velocity distribution, particularly above and below the assumed Moho. We display the resulting final velocity–depth model as a plot with contours of constant velocities to better illustrate the distribution of the velocity field (Fig. 6a). Superimposed on the velocity field are seismic boundaries derived from wide-angle reflections. Subhorizontal mid-crustal reflectors, 20 to 60 km long, occur at depths between 10 and 30 km. A series of north-dipping mid- to lower crustal reflectors were modelled in the southern part of the model. Their dip angles range
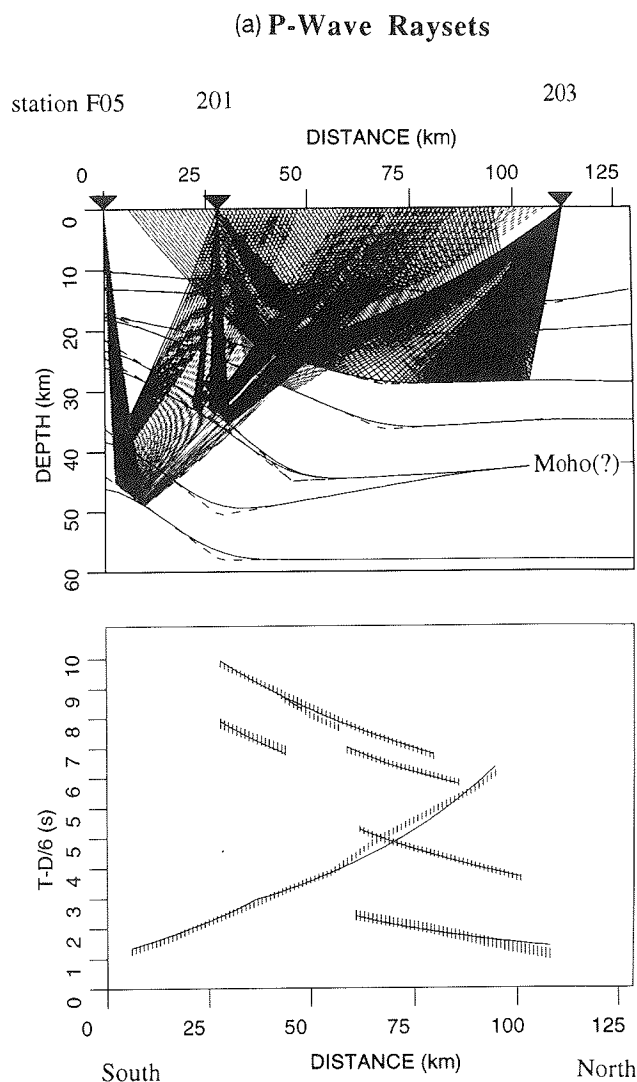

Figure 4. Examples of *P*-wave and *S*-wave ray sets used in the 2-D traveltime inversion. Heavy lines are the observed phases with picking uncertainties indicated by the line thickness. The thin lines mark calculated traveltimes. The inversion is based on a damped least-squares algorithm (Zelt & Smith 1992). Shown are the ray sets of (a) observed wide-angle reflections from north-dipping interfaces of the southern part of the model, (b) a lower crustal diving wave phase P_S, the Moho P_mP reflection and upper mantle P_n refraction arrivals, and (c) the Moho S_mS reflections and upper mantle S_n arrivals. The mismatch between the observed and calculated traveltimes of the SmS arrival of station F05 is probably a 3-D effect.

from 15° to 25°, increasing with greater depth. Two dipping reflectors reach depths of 50 km. We modelled the dominant, high-amplitude P_mP phases as reflections from an interface at 42 to 45 km depth assumed to be the Moho discontinuity (M) Near-surface velocities range between 5.7 and 5.8 km s^{-1} and reach up to 6.0 km s^{-1} in one part of the northern half of the model. Velocities increase steadily with depth and reach values of 6.4 to 6.6 km s^{-1} at about 20–25 km depth. A large vertical velocity gradient was modelled between 38 and 45 km depth. Velocities in that zone within the northern half increase from about 7.0 to
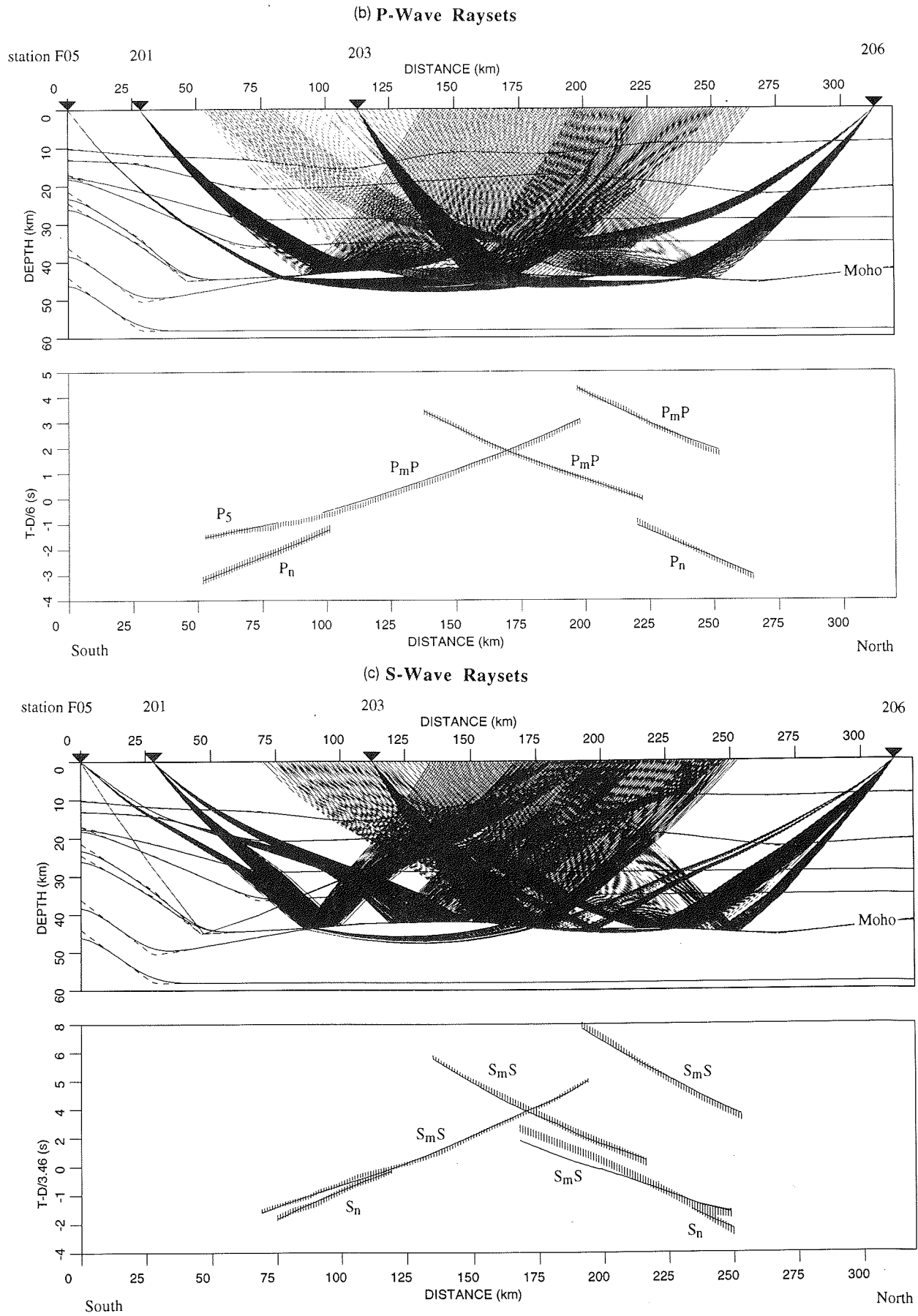
(b) P-Wave Raysets

(c) S-Wave Raysets
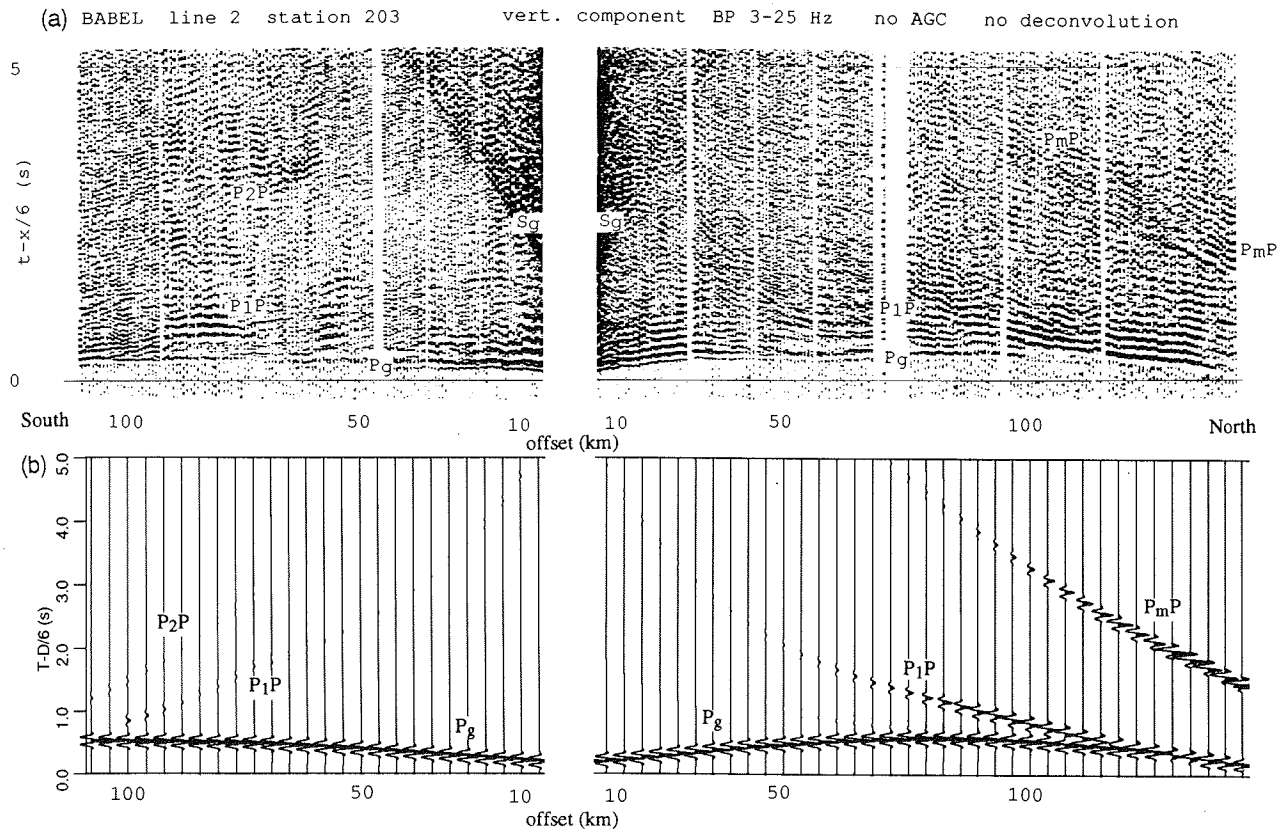

Figure 4. (*Continued*).

Figure 5. (a) Seismic section of station 203 without AGC and deconvolution applied and (b) the respective synthetic seismogram section. P_1P and P_2P denote upper to mid-crustal reflections.

$8.0\,\text{km s}^{-1}$ and up to $8.2\,\text{km s}^{-1}$ in one part of the model. The gradient is strongest right above the presumed Moho reflectors M_1 and M_2. In the southern part of the model, the velocity contours follow the dip direction of the reflectors which is partly an artefact due to the model parameterization in a zone of poor velocity control from large-offset reflections and/or refractions. The velocities in the lower mid-crust at about 35 km depth reach a minimum at about 80 km horizontal distance. A significant result is that the velocities below reflector M_2, between 80 and 150 km distance (7.6–$7.8\,\text{km s}^{-1}$), are lower than those in the northern half of the model (Fig. 6a).

We calculated the resolution of velocity and boundary nodes of the final model. The depths of reflectors shown in Fig. 6 are modelled within an uncertainty of about 2 km. We plotted the velocity resolution kernels on top of the depth model (Fig. 6b). For velocity nodes with resolution kernels larger than 0.5, the calculated velocity uncertainty is $<0.07\,\text{km s}^{-1}$. The distribution of zones of low and high resolution varies extremely. Zones of low ray coverage or those that contain only rays shot from a single direction (unreversed) exhibit low resolution, and vice versa. As expected with regard to the shot–profile/receiver geometry, the resolution kernels reach high values (about 0.8) in the upper crust of the southern half of the model due to a great density of overlapping, reversed rays of first arrivals (P_g). A number of overlapping and reversed rays from mid-crustal reflection and refraction phases keep the resolution to values above 0.5 in parts of the upper and middle crust.

Between 23 and about 42 km depth, the resolution is very poor, caused by the lack of reversed refracted or diving waves through the lower crust. The modelled velocities in that zone, therefore, might be not reliable and have to be interpreted with great caution. Also, because of the limited number of recording stations, the velocities in the region of the north-dipping reflectors are poorly resolved. The lack of refracted phases and the distribution of rays travelling to and reflecting off the dipping interfaces were not dense enough to build up higher velocity resolution kernels. The zone below the well-constrained Moho boundary again reaches higher resolution values of up to 0.6 due to observation of reversed P_n arrivals from stations F05 and 206. As mentioned above, the resolution values have to be regarded in a relative sense with respect to their distribution within the velocity model rather than in a sense of absolute values.

4.2 S-wave model

We modelled the S-wave velocity field by assuming similar depths for layer boundaries as in the P-wave model. Therefore, the boundary nodes were kept constant and we inverted only for velocities. The initial model contained velocities converted from the final P-wave model with a constant Poisson's ratio of 0.25. The calculated S-wave traveltimes of the initial model differed from the observed ones within reasonably small deviations, showing that our assumption of similar depths of seismic boundaries for
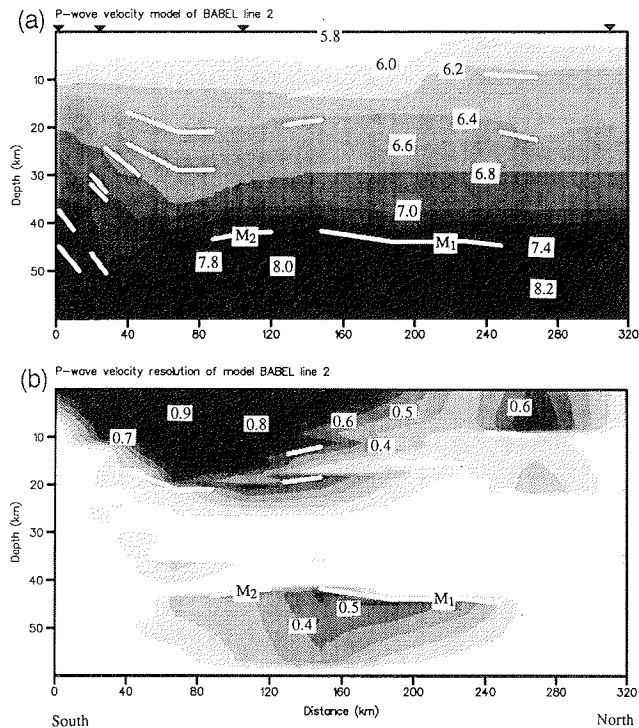
Figure 6. (a) *P*-wave velocity model (in km s^{-1}) and (b) its velocity resolution of a profile covering BABEL line 2. The model is the result of the 2-D traveltime inversion after linearily interpolating velocities between nodes. The white lines represent wide-angle *P*-wave reflectors. M_1 and M_2 mark the depth of Moho reflectors. Note the north-dipping mid- and lower crustal reflectors in the southern part of the profile. The resolution was calculated for all independent parameters within each individual layer while parameters outside the respective layer were kept constant. Contour interval for resolution kernels is 0.1. For velocity nodes with resolution kernels larger than 0.5, the calculated velocity uncertainty is <0.07 km s^{-1}. Velocities are best resolved in the upper crust to the south where station locations are denser and in parts of the upper mantle due to overlapping ray coverage of reversed P_n recordings. The poor velocity resolution in the middle and lower crust is caused by a lack of observed refracted and/or diving waves and the sparse station coverage.

P- and *S*-wave reflections was correct. Again we started inverting for velocities of the first layer and proceeded to the subsequent layers by keeping parameters of overlying layers fixed. The best RMS traveltime residuals were reached after a few iterations. The inversion kept stable with a few exceptions in which we had to adjust unreasonably high or low velocities manually. Most of the calculated traveltimes lie within the uncertainty bounds of the observed ones. Very good agreement was achieved for the S_mS and S_n arrivals (Fig. 4c), except for the S_mS phase of recording F04 which we were not able to fit accurately, possibly due to 3-D effects within the dipping zone and the offline position of that station.

The wide-angle reflections in the *S*-wave model (Fig. 7a) are less numerous than in the *P*-wave model, in particular in the zone of north-dipping interfaces. As for the *P*-wave model, mid-crustal reflectors and a long, continuous reflector at Moho depth (M) are observed. Velocities begin
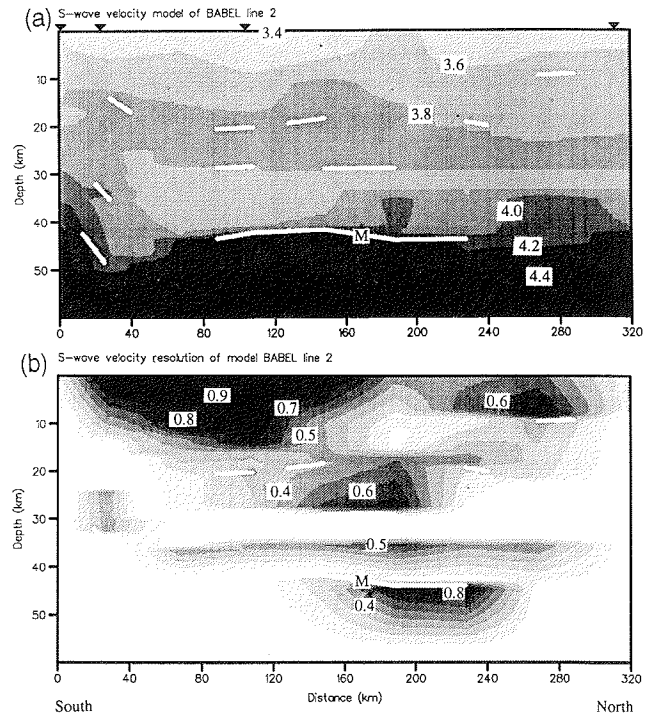

Figure 7. (a) *S*-wave velocity model (in km s^{-1}) and (b) its velocity resolution along BABEL profile 2. For explanation, see Fig. 6. M marks the depth of Moho reflectors. We assumed the same layer boundaries as for the *P*-wave model and inverted only for velocities. The white lines indicate wide-angle *S*-angle *S*-wave reflectors. For velocity nodes with resolution kernels larger than 0.5, the calculated velocity uncertainty is <0.07 km s^{-1}. As seen in the *P*-wave model, the resolution distribution illustrates the quality of the velocity field dependent on station coverage and observation of refracted and/or diving waves.

with 3.4 to 3.6 km s^{-1} in the uppermost crust and increase to about 3.9 km s^{-1} toward the middle crust. A zone of low velocities (3.7–3.8 km s^{-1}) in the lower crust was necessary to fit the S_mS arrivals into the given depth model. Obviously, direct velocity estimates cannot be obtained. Velocities reach values between 3.9 and 4.1 km s^{-1} at the base of the crust, assuming the reflector M is the Moho discontinuity. Below reflector M, velocities range between 4.2 and 4.4 km s^{-1}.

Similar to the *P*-wave velocity model, zones of higher velocity resolution occur in the upper crust, parts of the middle crust, and below the M reflector (Fig. 7b). A thin zone in the lower crust contains higher resolution values due to overlapping ray coverage of S_mS reflections. The distribution of zones of low and high resolution is slightly different from those in the *P*-wave model, because of different ray-path geometries between *P* and *S* waves.

4.3   Poisson's ratios

Given the results of the final *P*- and *S*-wave velocity models, we produced a plot of the Poisson's ratios along profile 2 (Fig. 8) to obtain more constraints on the physical rock properties in that part of the Baltic Shield. There is a large variation of Poisson's ratios from very low (0.21–0.25) in the uppermost crust to low to intermediate (0.22–0.27) in the

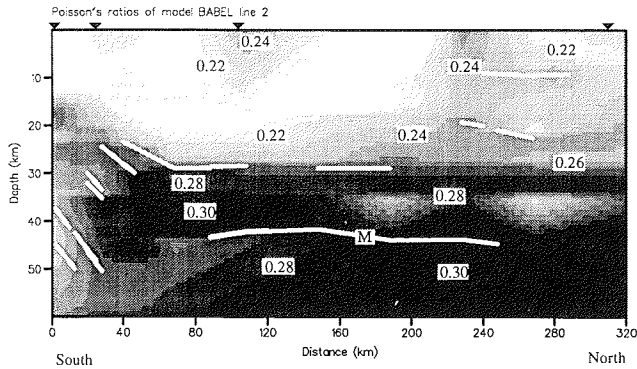**Figure 8.** Poisson's ratio model along BABEL profile 2 derived from the *P*- and *S*-wave models. The Poisson's ratios are to be evaluated with respect to velocity resolutions. Many of the Poisson's ratio 'anomalies' are probably artefacts due to low resolution of parts of the *P*- and *S*-wave velocity fields. The white lines represent combined wide-angle *P*- and *S*-wave reflectors. M marks the depth of Moho reflectors.

middle and lower mid-crust and values exceeding 0.30 in parts of the lower crust and upper mantle. At first sight, this distribution seems to be awkward. In parts of the model it is probably erroneous due to the low *P*- and *S*-wave velocity resolution. Uncertainties in *P*- and *S*-wave velocities of $0.2\,km\,s^{-1}$ at a single node can generate an uncertainty of up to 0.09 (!) in the Poisson's ratio in an extreme case. Therefore, only Poisson's ratios in zones with high resolution of both *P*- and *S*-wave velocities are reliable enough to be interpreted in terms of physical rock properties. In this regard, we place emphasis on ratios in zones with resolution kernels greater than 0.5. In these zones, Poisson's ratios are between 0.21 and 0.25 in the upper crust and about 0.30 in parts of the lowermost crust and uppermost mantle. These values do not take into account possible effects of seismic anisotropy.

4.4 Discussion of models

The velocity–depth models along profile 2 show some dominant and significant characteristics. First, there is the shape and distribution of wide-angle reflectors within the zone of north-dipping layer boundaries in the middle and lower crust of the southern end of the model, and the undulating shape of upper to mid-crustal as well as Moho reflectors. The reflectors in the dipping zone are almost parallel in the lower crust, and their dip angle becomes smaller in the middle crust. Their location coincides with that of the high-amplitude dipping reflectors between 28 and 37 km depth observed on a wide-angle multichannel array data set (station 202) by Lindsey & Snyder (1992). Due to the good quality and high resolution of the stacked multichannel data, Lindsey & Snyder (1992) were able to model this zone as a stack of fine-layered sequences. They interpreted it as a sequence of imbricated slices of underthrust oceanic crust intermixed with sediments, a laminated mylonite zone created by shear processes during collision, or a zone of mafic intrusives emplaced during subduction. Our velocity models show *P*-wave velocities of 6.8 to $7.3\,km\,s^{-1}$ and *S*-wave velocities of 3.8 to $4.2\,km\,s^{-1}$

in that zone between 25 and 40 km depth, indicating intermediate to mafic composition. The velocities, however, are not well resolved and should be interpreted cautiously. The question of whether this zone of dipping reflectors consists of metamorphosed oceanic crust or mafic intrusives cannot be answered by considering the velocity model.

The upper to middle crust is characterized by a bowl-like shape of the reflectors to the south and a dome-like form to the north. *P*-wave velocities of 5.7 to $6.0\,km\,s^{-1}$ in the subsurface indicate felsic to intermediate composition. Thick sedimentary sequences on top of the crystalline basement do not exist in this region of the Gulf of Bothnia, except for the 1.3 Ga old Jotnian Sandstone to the north (Ahlberg 1986) which produces a few reflections within the first second in the normal-incidence reflection data but cannot be imaged in our large-offset recordings. The slight drop in mid-crustal *P*-wave velocities in the southern part correlates with the bowl-shaped reflector structure and might indicate a basin-like formation of rocks with more felsic components. Velocities of 6.6 to $7.2\,km\,s^{-1}$ in the middle to lower crust north of the dipping zone are typical of Precambrian shields (i.e. Lyons, Forsyth & Mair 1980; Boland & Ellis 1989) and are generally interpreted as an increase in metamorphic grade and/or mafic components (Christensen & Fountain 1975; Burke & Fountain 1990), but their resolution is extremely poor. The extremely high velocities of up to $7.6\,km\,s^{-1}$ at the base of the crust indicate a granulite metamorphic grade and/or predominantly mafic composition.

The large velocity contrast of the layers above and below the M reflectors and the high *P*-wave felocities of greater than $8.0\,km\,s^{-1}$ below M_1 are evidence that reflector M_1 certainly represents the Moho discontinuity at 42 to 45 km depth. These Moho depths coincide with those modelled for the adjacent BABEL profiles 3 and 4 by Komminaho & Yliniemi (1992a,b). Reflector M_1 is located in line with M_2 and likely represents the Moho as well. The velocities below M_2, however, indicate that the material in the 'apparent' upper mantle between 43 and 50 km depth in the southern part of the profile contains more mafic than ultramafic components. This zone of low mantle velocites seems to appear in context with the formation of the north-dipping structures and might be a result of the collisional process.

Poisson's ratios between 0.21 and 0.25 for the upper crust indicate a dominantly felsic, quartz-rich composition. An increase of the Poisson's ratio with depth is the result of an *S*-wave velocity field that exhibits a small increase and—in the lower crust—even a decrease of velocities with depth compared to the *P*-wave model. Ward & Warner (1991) showed that increasing mafic composition with depth would explain such a behaviour of the *S*-wave velocity and Poisson's ratio fields. We suggest a lower crust of mafic, amphibolitic composition (Kern 1982) in parts along profile 2 due to Poisson's ratios locally exceeding 0.30. The lack of highly resolved velocities in other parts of the lower crust does not allow a more specific estimation of composition.

Conventional forward ray tracing often generates velocity models that are partly over-interpreted due to the lack of numerical control on model parameters. The display of resolution kernels calculated from an inversion routine provides better constraints on the model reliability despite the above-mentioned problems with two-dimensionality of

the used data set and non-linearity of the inverse problem. It is, in our case, striking that regions of well-resolved velocities are rather limited. Regions of poor or zero resolution do not necessarily have to contain erroneous velocities. Their velocities are good enough to fit the data of arrivals travelling through these zones, but only their averaged values over large areas of the 2-D model are meaningful. The high shot density of receiver gathers results in improved phase identification and traveltime estimation, but only combined dense shot *and* receiver locations in connection with large offset coverage will help improving the velocity resolution of wide-angle reflection and refraction models.

5 SEISMIC NORMAL-INCIDENCE DATA

We want to compare our velocity–depth model with the stacked CMP reflection data of profile 2. The wide-angle reflection midpoints do not exactly coincide with the common midpoints in most parts of the profile, but their

deviation is tolerable because the strike direction of the dominant geological boundaries is assumed perpendicular to the profile. The processing procedure of the CMP reflection data is described in detail by the BABEL Working Group (1993). The data were migrated using a finite-difference (FD) migration routine with velocities from the above-described velocity–depth model (Fig. 9a). Mainly for display purposes, but also as an interpretation aid, we applied a coherency filter to the stacked and migrated data. The filter is based on semblance calculation of a number of adjacent traces. We chose adjacent CDP traces within 900 m width and a maximum dip angle range of $\pm 30°$ (average crustal velocity of $6.5 \, km \, s^{-1}$ assumed) to include all coherent dipping reflections. In addition, a semblance weight function was applied to each sample.

The coherency-filtered stack (Fig. 9b) shows an improved image of areas of high and low reflectivity. Below a thin sedimentary sequence, the reflectivity in the upper 3 to 4 s is extremely low. Zones of high reflectivity occur in the middle crust and parts of the lower crust. The abrupt change from
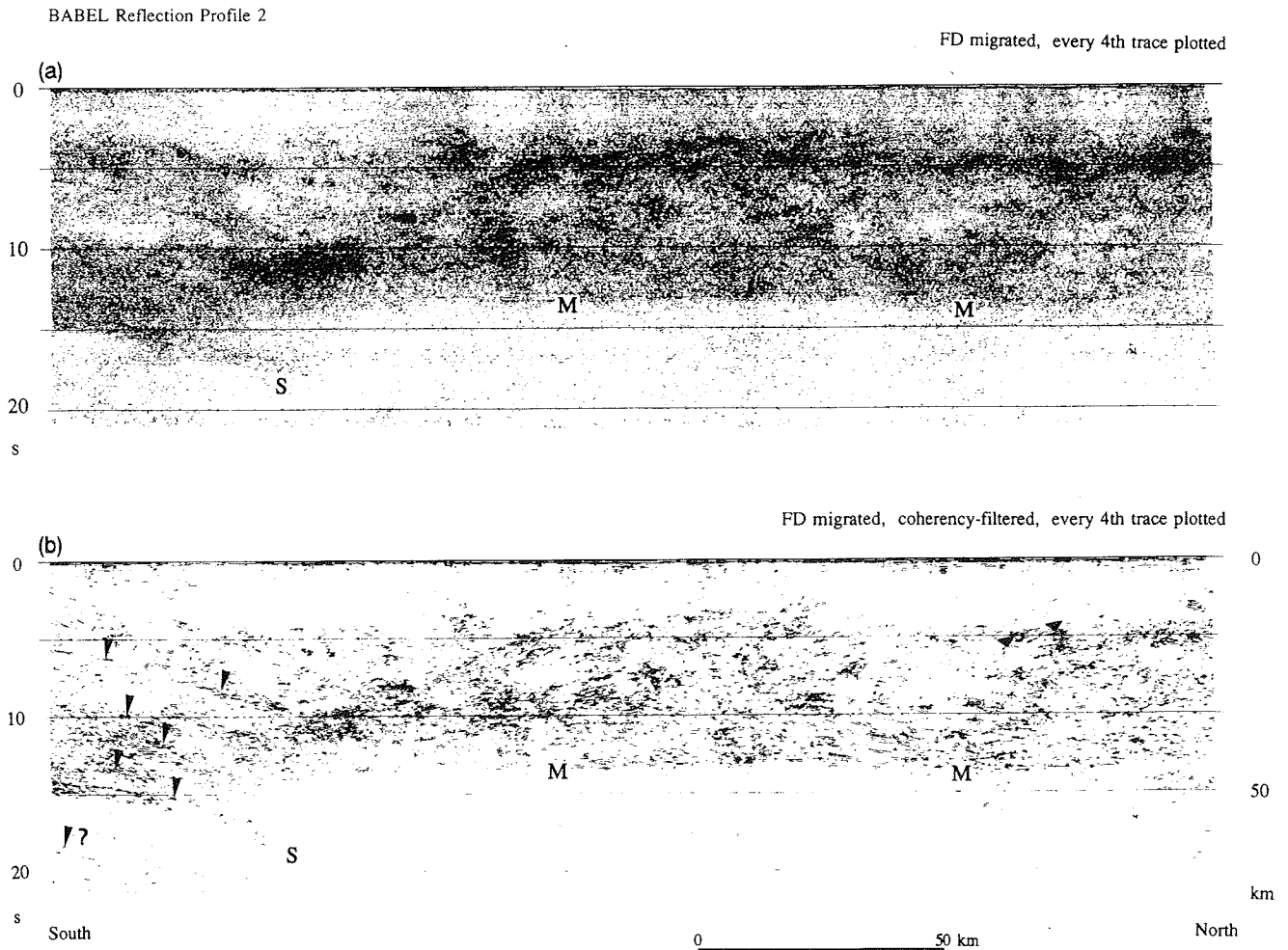

Figure 9. (a) CMP reflection data of BABEL profile 2. Data were processed by GECO-PRAKLA, Hannover, and migrated by BIRPS, University of Cambridge. (b) We applied a coherency filter with a semblance weight function to suppress incoherent noise and enhance zones of high reflectivity. M marks the Moho, and S indicates the interpreted Proterozoic subduction slab (BABEL Working Group 1990, 1993). Long arrows mark series of prominent north-dipping reflectors; short arrows mark slightly south-dipping reflectors in the northern part of the profile.

reflective to transparent characteristics at 13.5 to 14.5 s in the central part is consistent with the location of the M reflectors at 42 to 45 km depth in the wide-angle analysis. It marks clearly the crust–mantle boundary. A continuous Moho reflector, however, is not observed, unlike in the neighbouring BABEL profiles 3 and 4 (BABEL Working Group 1993). Thick Moho transition zones with lithological and metamorphic layering have been suggested for many Precambrian cratons based on the high reflectivity in the lowermost crust but lack of continuous Moho reflectors (Mooney & Meissner 1992). The depth to the crust–mantle boundary remains constant in the central part of the profile and seems to increase slightly northward where the reflections become blurred. At the southern end of the profile, a strong band of reflections occurs at about 15 s (50 km depth). It continues dipping northward into the upper mantle with an angle increasing to about 30° (an average crustal velocity of 6.5 km s^{-1} is assumed). The same type of dipping reflector is observed on profile 4, almost parallel to profile 2 (Fig. 1), where it can be traced down to about 25 s. There, it contains even higher amplitudes and is more coherent than in profile 2. Authors of previous papers have already described these mantle reflectors in the northern Gulf of Bothnia and interpreted them as relics of a subducted oceanic (?) crust emplaced during Proterozoic collision (BABEL Working Group 1990, 1991, 1993). Although amplitudes from the crust–mantle boundary at the southern end of profile 2 are high and the reflectors are continuous, neither we in our single station wide-angle data nor Lindsey & Snyder (1992) in their multichannel wide-angle data observe such a distinct boundary at the same location as in the CMP data. The series of north-dipping wide-angle reflectors down to 50 km depth were modelled just south of the end of profile 2. There is a hint of another set of north-dipping mantle reflections at the southern edge of the profile that line up with the dipping wide-angle reflectors. More clearly coinciding with the dipping wide-angle reflectors is the zone of north-dipping normal-incidence reflections between 6 and 11 s (21–35 km depth).

The zone of north-dipping reflectors is interrupted in the south-central part of the profile where an area of high-amplitude, coherent reflections is concentrated in the mid- to lower crust. The reflectors of that zone are subhorizontal without a predominant dip direction. This reflective zone thickens northward in a wedge-like shape occupying most of the middle crust (3–11 s) in the central section of the profile. Coinciding with reflection bands in the upper part of this reflective zone are the modelled wide-angle *P*-and *S*-wave reflectors between 9 and 30 km depth. In fact, the lower boundary of that zone is identical with the location of the *S*-wave reflector at 30 km depth in the centre of the velocity–depth model (Fig. 7a). Farther north, the mid-crustal reflectivity decreases over a region of about 30 km length before it reappears in the northern part of the profile. This northward increase of mid- to lower crustal reflectivity again is developed within a wedge-shaped structure.

Many previously recorded reflection profiles over Precambrian crust show preferences for either upper or lower crustal reflectivity and, in most cases, a lack of distinct Moho reflections or sudden change in reflectivity at the crust–mantle boundary (Smithson *et al.* 1987). Although reflection profile 2 and many of the other BABEL profiles over Precambrian crust exhibit great variations in reflectivity characteristics, they generally show a uniform appearance of a reflective upper middle to lower crust. The Svecofennian in the northern Gulf of Bothnia region has not experienced any major tectonic activities since the Sveconorwegian–Grenvillian orogeny (1.25–0.9 Ga) and was only slightly affected by the Caledonian orogeny (0.6–0.4 Ga) (Gorbatschev & Gaál 1987). Therefore, expressions of younger tectonic activity such as shear zones and major intrusions that might have overprinted the pre-existing structure are not expected to occur. That leaves us a chance to observe, delineate and interpret seismic signals from a predominantly Precambrian structure. The constant source and receiver parameters of a marine experiment and a thin sedimentary cover minimize acquisition-related disturbing factors that exist in many land surveys.

6 SUGGESTION FOR A GEOLOGICAL CROSS-SECTION

In combining geological surface information with the results from our velocity–depth and Poisson's ratio models, seismic reflection profile 2, and other geophysical information from the Gulf of Bothnia region, we attempted to construct a simplified geological cross-section along BABEL profile 2 (Fig. 10). We want to focus on two major aspects that describe the collisional characteristics of the Proterozoic Svecofennian and the Archaean provinces. The first is associated with the north-dipping reflectors and the already-suggested Proterozoic subduction. The second is the location of the Proterozoic–Archaean boundary and the occurrence of south-dipping zones in the northern part of the Bothnian Bay.

There is geological as well as geophysical evidence for a possible subduction process in the Proterozoic, as already pointed out in previous papers by the BABEL Working Group (1990, 1991, 1993). The abundance of synorogenic granitic plutons exposed on the Swedish and Finnish side of the Bothnian Bay and the metavolcanic/metasedimentary character of the CSP led to the suggestion that a volcanic (island) arc complex was formed at the southern edge of the Archaean craton (Skiöld & Öhlander 1989; Gaál 1990). Both reflection profiles 2 and 4 and the velocity–depth models show strong, coherent upper-mantle reflectors that continue upward into the lower crust where they are accompanied by series of north-dipping, high-amplitude reflectors. There is no direct evidence for oceanic crustal material in the lower crust or upper mantle from the seismic data and velocity profiles, but other features in the reflection and velocity profiles provide indirect indications for one or, possibly, two or more subducted oceanic slabs.

Because of their thickness of several kilometres and the high amplitudes of their reflectors, the zones of dipping interfaces might be related to a diving slab of oceanic crust. We agree with one of Lindsey & Snyder's (1992) interpretations in which this zone might consist of imbricated or intercalated mafic and sedimentary sequences that were scraped off the oceanic plate during the subduction process and stacked on top of a remnant oceanic plate. A large acoustic impedance contrast between slices of

Schematic Geological Cross-Section Along BABEL Profile 2

Southwest   Northeast
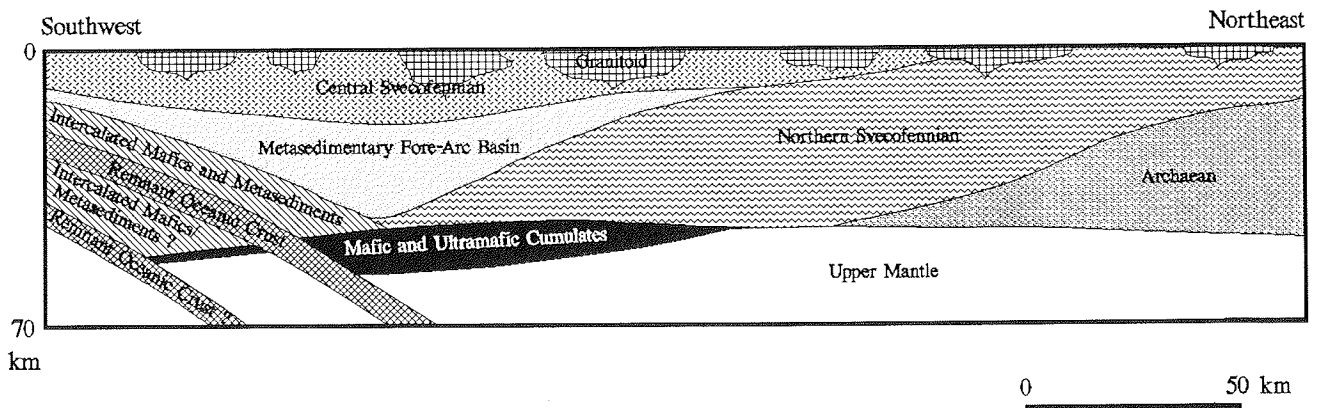

Figure 10. Schematic geological cross-section along BABEL profile 2 derived from seismic velocity models and CMP reflection data. See text for explanation.

deformed sedimentary rocks and oceanic mafic rocks would explain the high-amplitude reflections.

The normal-incidence data of profiles 2 and 4 show hints of upper mantle reflections at their southernmost ends parallel to the dominant north-dipping mantle reflectors. Unfortunately, the profiles do not extend farther south-west to observe the southward and upward continuation of these reflections, but we speculate that they might be generated from another down-dipping slab of possible oceanic crustal material. Such a sequence of multiple subducted slabs has been observed in regions of currently ongoing subduction processes and are explained by a subsequent breakup of the primary slab and continuation of the subduction at a different position (Clowes et al. 1987). The space between both slabs might be filled with an imbricated mixture of metasediments and mafic rocks, similar to those on top of the primary slice of remnant oceanic crust.

The basin-shaped structure above the northern end of the north-dipping mid-crustal reflectors is characterized by relatively low reflectivity and slightly lower P-wave velocities than in its lateral surroundings. Its geometrical shape, velocities, and location on top of the subduction slab imply a possible fore-arc basin filled with oceanic and island-arc related sediments, such as greywackes, that were metamorphosed and intruded by synorogenic plutons. Such a remnant of a Proterozoic metasedimentary fore-arc basin has already been suggested by the BABEL Working Group (1990), and our evidence in the velocity distribution supports their interpretation.

The unusually low velocities (7.6–7.8 km s^{-1}) in the zone above the dominant mantle reflectors and below the presumed Moho indicate that it does not consist exclusively of typical ultramafic mantle rocks. Our preferred interpretation of this zone is that it comprises a mixture of mafic to ultramafic cumulates, generated from differentiation processes during subduction. Layers of underplated mantle-derived material have been widely postulated in extensional regimes (i.e. Furlong & Fountain 1986; Fountain 1989) and are suspected in subduction-related compressional regimes as well. For instance, Kay & Kay (1985) deduced the existence of a mafic to ultramafic zone at the crustal base of

the Aleutian arc from analyses of xenolith samples. A gradual increase in ultramafic components and seismic velocities with depth would cause the lack of distinct reflections from the base of that zone as observed on profile 2.

By following the dominant reflectivity pattern of reflection profile 2, we drew the south-dipping boundaries of the NSP and the Archaean province. The reflection profile crosses the Archaean palaeoboundary inferred from isotopic studies (Öhlander et al. 1993). The upper envelope of the reflective mid-crustal wedge that forms the boundary of the presumed metasedimentary fore-arc basin correlates with the exposed intra-Svecofennian boundary when it is interpolated through the upper crustal zone of low reflectivity. A direct correlation with the Province boundaries is not possible because of the lack of continuous reflectors in the upper 2 to 3 s of the reflection data, possibly related to granitic plutons in the upper crust. We infer that the entire wedge and most of the reflective middle and lower crust in the centre of the profile might belong to the NSP. The northern part of the zone interpreted as the NSP is bounded by another zone of south-dipping reflectors in the middle crust. The profile does not cross parts of the Archaean according to geological surface observations, but it was already suspected earlier that the Archaean Province extends underneath the NSP (Öhlander et al. 1993). We speculate that this northern mid-crustal reflective zone might be part of the Archaean Province. BABEL profile 3 contains more distinct south-dipping reflectors in its northern part (BABEL Working Group 1993), suggesting that perhaps older collisional activities generated that boundary whose strike is significantly different from that of the southern reflectivity patterns.

The BABEL Working Group (1993) interpreted the reflectivity patterns in the northern parts of profiles 2 and 3 as the boundary zone between the Svecofennian volcanic arc, with volcanites causing the subhorizontal band of reflections between 4 and 5 s two-way time in the CDP data, and the underlying Archean basement. Based solely on the reflectivity patterns of our coherency-filtered reflection data, we would agree with their interpretation. However, our

velocity models do not show any variations in velocity distribution between the crustal blocks. We observe uniform *P*- and *S*-wave velocity fields and similar Moho depths for both the Proterozoic Svecofennian Province and the suggested Archean block. Only toward the northern end of profile 2 do the Moho depths increase to about 50 km.

Our geological model for the Bothnian Bay is very simplified but serves to show some large-scale crustal features of the Proterozoic–Archaean collision in the Baltic Shield. Much of the interpretation is constrained by the seismic reflection data and velocity profiles, supported by geological surface observations. There are also some pure speculations due to a lack of geological and geophysical data, but we have tried to place them in reasonable geological context.

7   CONCLUSIONS

Combined seismic CMP reflection and wide-angle reflection and refraction experiments such as the BABEL project provide the opportunity to derive seismic velocity fields parallel or in close proximity to the structures observed in the normal-incidence recording. BABEL profile 2 extends from the presumed magmatic arc complexes of the Proterozoic CSP to the NSP and crosses the boundary to the Archean cration of the northern Baltic Shield inferred from isotopic studies. We analysed the three-component recordings of the wide-angle seismic experiment, derived a velocity–depth model, compared the results with the CMP profiling, and developed a geological model of the Proterozoic–Archaean crust for the northern Gulf of Bothnia that illustrates the results of plate collisional events in the Proterozoic.

Results from 2-D traveltime inversion show a series of north-dipping reflectors in the middle and lower crust toward the southern end of the profile, as indicated by large move-out wide-angle reflections. We modelled several subhorizontal upper to mid-crustal reflectors and strong Moho reflectors at 42 to 45.km depth in the central part of the profile. *P*-wave velocities increase from about 5.7 km s^{-1} at the near-surface to 6.4–6.6 km s^{-1} in the middle crust. The lowermost crust contains a large velocity gradient with velocities of up to 7.6 km s^{-1}. P_n velocities reach 8.0 to 8.2 km s^{-1} up to 7–8 km below the Moho reflectors in the northern part of the model, but are under 8.0 km s^{-1} for the same depth range in the southern half. Poisson's ratios, calculated from the *P*- and *S*-wave models, range from 0.21 to 0.25 in the uppermost crust to about 0.30 in the lower crust and upper mantle. In parts of the middle and lower crust, we derived interpretations based on velocities with great caution due to low resolution of the velocity nodes. Our velocity and Poisson's ratio models indicate that the upper crust contains predominantly felsic, quartz-rich rocks such as granites and granitic gneisses. The increase of *P*-wave velocity and Poisson's ratio in the mid- and lower crust is explained by increasingly mafic composition. Parts of the lower crust along the profile may consist of amphibolites.

By comparing results of the velocity–depth model with the migrated and coherency-filtered CMP stack, we find that most of the wide-angle reflectors coincide with zones of high reflectivity or an abrupt change of reflextivity character in the CMP data. Some of the dominant characteristics of the CMP data are a zero of north-dipping reflectors in the southern part, north-dipping upper mantle reflectors at about 70 km depth, and zones of high reflectivity in parts of the upper and lower crust. Dinstinct Moho reflections are not observed, but the Moho is well defined by an abrupt loss of reflectivity. The Moho depth from the CMP data is consistent with that of the wide-angle model.

In agreement with previous suggestions by the BABEL Working Group (1990, 1991, 1993) and Lindsey & Snyder (1992), we interpret the zone of north-dipping reflectors as part of a remnant slab of possibly oceanic crustal composition with overlying imbricated metasediments and mafic rocks that were scraped off a descending oceanic crust. There are hints of another segment of subducted crust at the southernmost end of profile 2. This would suggest a multiple subduction process in which the slab broke into two or even more segments descending at different locations. We interpret the basin-shape geometry of a low-reflectivity zone with relatively low velocities in the middle crust above the presumed subducted slab as a former fore-arc basin that underwent metamorphism and intrusions by synorogenic plutons. It is possible that the subduction led to differentiation processes generating cumulates of mafic to ultramafic rocks beneath the crust on top of the subducting slab as indicated by the anomalously low P_n velocities (<8.0 km s^{-1}) beneath the Moho. There is no interpreted difference in the velocity distribution between Proterozoic and Archaean provinces, but patterns of low and high reflectivity follow a south-dipping trend in the northern part of the profile and are interpreted as boundaries between the Svecofennian and Archaean provinces. The Archaean probably extends in a wedge-like shape underneath the NSP in the middle and lower crust. Adjacent BABEL profile 3 contains more profound south-dipping reflectors in the northern Bothnian Bay (BABEL Working Group 1993), suggesting that perhaps older collisional activities generated that boundary whose strike is significantly different from that of the southern reflectivity patterns. It is possible that earlier collisional phases or events created south-dipping shear zones.

Despite the 3-D character of the wide-angle shot–receiver geometry in many places, our 2-D inversion model serves as a valuable approximation, because results from reflection profiles 2, 3 and 4 indicate that most geological boundaries strike almost perpendicular to the profiles. It is, however, desirable for the future, when reliable and efficient 3-D inversion routines are available, to include all wide-angle recordings in the Gulf of Bothnia region in an analysis to construct a highly resolved 3-D block image of this complex collisional crustal region.

computer facilities and time. Pekka Heikkinen provided the recordings of the Finnish land-stations. The CMP reflection data were processed by GECO-PRAKLA and migrated by BIRPS. Scott B. Smithson and an anonymous reviewer provided valuable criticism and comments on the submitted manuscript.

REFERENCES

Ahlberg, P., 1986. Den svenska kontinentalsockelns berggrund, *Sveriges geol. unders.*, Report **47**.

BABEL Working Group, 1990. Evidence for early Proterozoic plate tectonics from seismic reflection profiles in the Baltic shield, *Nature*, **348**, 34–38.

BABEL Working Group, 1991. Reflectivity of a Proterozoic shield: Examples from BABEL seismic profiles across Fennoscandia, in *Continental Lithosphere: Deep Seismic Reflections*, pp. 77–86, eds Meissner, R., Brown, L., Dürrbaum, H.-J., Franke, W., Fuchs, K. & Seifert, F., Geodyn. Ser. 22, Am. geophys. Un., Washington, DC.

BABEL Working Group, 1993. Integrated seismic studies of the Baltic shield using data in the Gulf of Bothnia region, *Geophys. J. Int.*, **112**, 305–324.

Berthelsen, A., 1984. The tectonic division of the Baltic shield, in *Proceedings of the First Workshop on the European Geotraverse, The Northern Segment*, pp. 13–22, eds Galson, D.A. & Mueller, St., European Science Foundation, Strasbourg.

Boland, A.V. & Ellis, R.M., 1989. Velocity structure of the Kapuskasing Uplift, Northern Ontario, from seismic refraction studies, *J. geophys. Res.*, **94**, 7189–7204.

Burke, M.M. & Fountain, D.M., 1990. Seismic properties of rocks from an exposure of extended continental crust—new laboratory measurements from the Ivrea Zone, *Tectonophysics*, **182**, 119–146.

Christensen, N.I. & Fountain, D.M., 1975. Constitution of the lower continental crust based on experimental studies of seismic velocities in granulite, *Geol. Soc. Am. Bull.*, **86**, 227–236.

Claesson, L.-Å., 1985. The geochemistry of early Proterozoic metavolcanic rocks hosting massive sulphide deposits in the Skellefte district, northern Sweden, *J. geol. Soc. Lond.*, **142**, 899–909.

Clowes, R.M., Brandon, M.T., Green, A.G., Yorath, C.J., Sutherland Brown, A., Kanasewich, E.R. & Spencer, C., 1987. LITHOPROBE—southern Vancouver Island: Cenozoic subduction complex imaged by deep seismic reflection, *Can. J. Earth Sci.*, **24**, 31–51.

Fountain, D.M., 1989. Growth and modification of lower continental crust in extended terrains: The role of extension and magmatic underplating, in *Properties and Processes of Earth's Lower Crust*, pp. 287–299, eds Mereu, R.F., Mueller, St. & Fountain, D.M., Am. geophys. Un., Geophys. Monogr. 51, IUGG Volume 6.

Front, K. & Nurmi, P.A., 1987. Characteristics and geological setting of syn-kinematic Svecokarelian granitoids in southern Finland, *Precambrian Res.*, **35**, 207–224.

Furlong, K.P. & Fountain, D.M., 1986. Continental crustal underplating: thermal considerations and seismic-petrologic consequences, *J. geophys. Res.*, **91**, 8285–8294.

Gaál, G., 1986. 2200 million years of crustal evolution: the Baltic shield, *Bull. geol. Soc. Finland*, **58**, 149–168.

Gaál, G., 1990. Tectonic styles of Early Proterozoic ore deposition in the Fennoscandian Shield, *Precambrian Res.*, **46**, 83–114.

Gaál, G. & Gorbatschev, R., 1987. An outline of the Precambrian evolution of the Baltic shield, *Precambrian Res.*, **35**, 15–52.

Gohl, K. & Pedersen, L.B., 1992. Archaean and Early Proterozoic units around northern Gulf of Bothnia: Interpretation of wide-angle data from Sweden, in *The BABEL Project: First Status Report*, pp. 47–50, eds Meissner, R., Snyder, D., Balling, N. & Staroste, E., Commission of the European Communities, Directorate-General XII, Brussels.

Gorbatschev, R. & Gaál, G., 1987. The Precambrian history of the Baltic shield, in *Proterozoic Lithospheric Evolution*, pp. 149–158, ed Kröner, A., Geodyn. Ser. 17, Am. geophys. Un., Washington, DC.

Guggisberg, B., Kaminski, W. & Prodehl, C., 1991. Crustal structure of the Fennoscandian Shield: A traveltime interpretation of the long-range FENNOLORA seismic refraction profile, *Tectonophysics*, **195**, 105–137.

Henkel, H., Lee, M.K. & Lund, C.-E., 1990. An integrated geophysical interpretation of the 200 km FENNOLORA section of the Baltic shield, in *The European Geotraverse: Integrative Studies*, pp. 1–47, eds Freeman, R., Giese, P. & Mueller, St., European Science Foundation, Strasbourg.

Hirschleber, H., Lund, C.-E., Meissner, R., Vogel, A. & Weinrebe, W., 1975. Seismic investigations along the Scandinavian "Blue Road" traverse, *J. Geophys.*, **41**, 135–148.

Kay, S.M. & Kay, R.W., 1985. Role of crystal cumulates and the oceanic crust in the formation of the lower crust of the Aleutian arc, *Geology*, **13**, 461–464.

Kern, H., 1982. Elastic-wave velocity in crustal and mantle rocks at high pressure and temperature: the role of high-low quartz transition and of dehydration reactions, *Phys. Earth planet. Inter.*, **29**, 12–23.

Komminaho, K. & Yliniemi, Y., 1992a. Archaean and Early Proterozoic units around northern Gulf of Bothnia: Interpretation of wide-angle data from Finland, in *The BABEL Project: First Status Report*, pp. 51–53, eds Meissner, R., Snyder, D., Balling, N. & Staroste, E., Commission of the European Communities, Directorate-General XII, Brussels.

Komminaho, K. & Yliniemi, Y., 1992b. Combined interpretation of *P*- and *S*-wave data along the BABEL lines 3 and 4 in the northern part of the Gulf of Bothnia, in *The BABEL Project: First Status Report*, pp. 55–58, eds Meissner, R., Snyder, D., Balling, N. & Staroste, E., Commission of the European Communities, Directorate-General XII, Brussels.

Korsmann, K., ed., 1988. Tectono-metamorphic evolution of the Raahe–Ladoga zone, eastern Finland, *Bull. geol. Surv. Finland*, **343**.

Lindsey, G. & Snyder, D.B., 1992. Pre-critical wide-angle reflections on BABEL line 2: images of a 1.8 Ga suture zone, in *The BABEL Project: First Status Report*, pp. 41–46, eds Meissner R., Snyder, D., Balling, N. & Staroste, E., Commission of the European Communities, Directorate-General XII, Brussels.

Lundberg, B., 1980. Aspects of the geology of the Skellefte field, northern Sweden, *Geol. Fören. Stockholm Förh.*, **102**, 156–166.

Lundström, I., 1987. Lateral variations in supracrustal geology within the Swedish part of the southern Svecofennian volcanic belt, *Precambrian Res.*, **35**, 353–365.

Lyons, J.A., Forsyth, D.A. & Mair, J.A., 1980. Crustal studies in the La Malbaie Region, Quebec, *Can. J. Earth Sci.*, **17**, 478–490.

Meissner, R., 1986. *The Continental Crust*, Academic Press, Orlando.

Mooney, W. D. & Meissner, R., 1992. Multi-genetic origin of crustal reflectivity: a review of seismic reflectivity profiling of the continental lower crust and Moho, in *Continental Lower Crust*, pp. 45–79, eds Fountain, D.M., Arculus, R. & Kay, R.W., Elsevier, Amsterdam.

Öhlander, B., Skiöld, T., Elming, S.-Å., Claesson, S., Nisca, D.H. & BABEL Working Group, 1993. Delineation and character of

the Archaean–Proterozoic boundary in northern Sweden, *Precambrian Res.,* **64,** 67–84.

Park, A.F., 1991. Continental growth by accretion: a tectonostrati-graphic terrane analysis of the evolution of the western and central Baltic shield, 2.50 to 1.75 Ga, *Geol. Soc. Am. Bull.,* **103,** 522–537.

Patchett, P.J., Todt, W. & Gorbatschev, R., 1987. Origin of continental crust of 1.9–1.7 Ga age: Nd isotopes in the Svecofennian orogenic terrains of Sweden, *Precambrian Res.,* **35,** 145–160.

Rasmussen, T.M., Roberts, R.G. & Pedersen, L.B., 1987. Magnetotellurics along the Fennoscandian Long Range profile, *Geophys. J. R. astr. Soc.,* **89,** 799–820.

Skiöld, T. & Öhlander, B., 1989. Chronology and geochemistry of late Svecofennian processes in northern Sweden, *Geol. Fören. Stockholm Förh.,* **111,** 347–354.

Smithson, S.B., Johnson, R.A., Hurich, C.A., Valasek, P.A. & Branch, C., 1987. Deep crustal structure and genesis from contrasting reflection patterns: an integrated approach, *Geophys. J. R. astr. Soc.,* **89,** 67–72.

Ward, G. & Warner, M., 1991. Lower crustal lithology from shear wave seismic reflection data, in *Continental Lithosphere: Deep Seismic Reflections,* pp. 343–349, eds Meissner, R., Brown, L., Dürrbaum, H.-J., Franke, W., Fuchs, K. & Seifert, F., Geodyn. Ser. 22, Am. geophys. Un., Washington, DC.

Windley, B.F., 1984. *The Evolving Continents,* 2nd edn, Wiley, New York.

Zelt, C.A. & Ellis, R.M., 1988. Practical and efficient ray tracing in two-dimensional media for rapid traveltime and amplitude forward modelling, *Can. J. expl. Geophys.,* **24,** 16–31.

Zelt, C.A. & Smith, R.B., 1992. Seismic traveltime inversion for 2-D crustal velocity structure, *Geophys. J. Int.,* **108,** 16–34.